LINKING BRAIN ENTROPY TO MOLECULAR AND CELLULAR ARCHITECTURE IN PSYCHOSIS

Qiang Li[1], *Jingyu Liu*[1,2], *Vince D. Calhoun*[1,2] *Fellow, IEEE*

[1]Tri-Institutional Center for Translational Research in Neuroimaging and Data Science (TReNDS), Georgia State, Georgia Tech, and Emory University, Atlanta, GA, United States
[2]Department of Computer Science, Georgia State University, Atlanta, GA, United States

ABSTRACT

Brain entropy reflects the complexity of intrinsic activity and has been associated with cognitive function and psychiatric disorders. However, its relationship with neurochemical and cellular architecture in the brain remains poorly understood. By integrating molecular imaging, and neuroimaging datasets, we provide converging evidence that the spatial distribution of diverse cell types, neurotransmitter systems, and mitochondrial phenotypes is systematically associated with brain entropy. We found significant differences in entropy correlations between normal controls and individuals with schizophrenia for the mu-opioid receptor and dopamine receptor (D1), and between normal controls and bipolar disorder for the norepinephrine transporter (NAT) and N-methyl-D-aspartate receptor (NMDA). No significant differences were observed between schizophrenia and bipolar disorder in the neurotransmitter domain. In terms of cellular and metabolic features, both the normal controls vs. schizophrenia and normal controls vs. bipolar disorder comparisons revealed widespread differences associated with most mitochondrial markers, as well as glial cells and inhibitory neurons. These findings suggest disruptions in energy metabolism, neuroinflammatory activity, and inhibitory neuronal regulation in the clinical groups. Furthermore, these results indicate that brain entropy is not randomly distributed but is systematically linked to specific neurochemical systems and cellular characteristics. This systems-level perspective offers valuable insights into how the complexity of brain activity emerges from the underlying molecular architecture and how it is altered in psychiatric disorders. Moreover, it provides a biological foundation for understanding brain entropy in the context of psychosis.

Index Terms— Brain entropy, psychiatric disorders, molecular imaging, neurochemical and cellular architecture, biological foundation

1 Introduction

Brain entropy, when conceptualized as a component of complex dynamical systems such as the primate brain, quantifies the rate at which information is generated over time. One of the most commonly used estimators of complexity associated with entropy is *sample entropy* (SampEn) [1]. SampEn quantifies the unpredictability or irregularity of a time series by examining the probability of similar patterns within the data, given a known prior probabilistic distribution [1]. SampEn has been widely applied in the analysis of neuroimaging and physiological time series to assess the complexity of signals [2, 3, 4].

In addition to brain entropy measures derived from neuroimaging techniques like resting-state fMRI (rsfMRI), examining the spatial distribution of neurotransmitter systems and cell types is essential for a comprehensive understanding of brain function [5, 6, 7, 8]. Neurotransmitter maps, for instance, provide valuable insights into the density and distribution of critical neurochemical systems that underpin brain function and behavior. These maps not only help characterize normal brain function but also reveal how disruptions in neurotransmitter signaling may contribute to the pathophysiology of psychiatric disorders, such as schizophrenia (SZ) and bipolar disorder (BP) [9, 10]. Furthermore, exploring the distribution of various cell types such as glial, neuronal, and mitochondrial populations offers deeper insights into the brain's cellular architecture [6, 7, 8]. The interplay between these components and brain entropy can shed light on how alterations in cellular and neurochemical organization are linked to neural abnormalities observed in psychiatric conditions, potentially contributing to changes in brain entropy itself.

Together, neurotransmitter and cell-type maps, in conjunction with brain entropy analysis, offer a powerful approach to studying the complex biological mechanisms underlying psychosis and other neuropsychiatric disorders. This multidimensional perspective allows for a more nuanced understanding of how alterations in brain activity complexity might be linked to cellular and neurochemical disturbances, providing potential biomarkers for diagnosis and therapeutic targets.

2 Materials and methods

2.1 Participants

A total of 1432 participants were selected from the Bipolar and Schizophrenia Network for Intermediate Phenotypes (BSNIP) consortium [11]. This cohort included 640 healthy controls (NC), 470 individuals diagnosed with SZ, and 322 individuals with BP. Detailed demographic and clinical in-

formation about the participants is available in prior publications [11, 12]. Ethical approval was obtained by the contributing institutions, and all participants provided written informed consent.

2.2 MRI Data Acquisition and Preprocessing

Our rsfMRI data underwent a rigorous preprocessing pipeline to ensure data integrity and analytic reliability. The process began with stringent quality control to identify and retain only high-quality datasets. Subsequently, each participant's rsfMRI data were processed using a standardized pipeline that included rigid body motion correction, slice timing correction, and distortion correction. The data were registered to a common MNI space, resampled to isotropic voxels of 3mm^3, and smoothed using a Gaussian kernel with a full width at half maximum (FWHM) of 6mm.

2.3 Assessing Brain Signal Complexity via SampEn Measures

SampEn quantifies the complexity of the signal by measuring the negative natural logarithm of the conditional probability that two sequences similar for m consecutive points remain similar at the next point, within a tolerance r [1]. The tolerance r typically defines the maximum allowed distance for two points to be considered similar, commonly set to $0.2 \times \mathrm{std}(X)$, where std denotes the standard deviation of the time series. In contrast to related measures, SampEn excludes self-matches and produces more consistent results for shorter time series. In our case, we used parameters $m = 3$ and $r = 0.3$, corresponding to the embedding dimension and similarity tolerance, respectively. Importantly, SampEn is always non-negative, as it is defined as the negative logarithm of a conditional probability.

In the context of rsfMRI signals, the time series data can be represented by a set of observations, $x(i)$, where i represents the time point, and $x(i)$ is the signal value at the corresponding voxel at that time point. Given a time series of length T, we define a template vector of length l as:

$$X_l(i) = \{x_i, x_{i+1}, x_{i+2}, \ldots, x_{i+l-1}\}$$

This template vector represents a portion of the fMRI time series, and its structure is used to analyze the underlying complexity of brain activity. The distance function $\mathscr{D}[X_l(i), X_l(j)]$ is used to quantify the dissimilarity between two such vectors $X_l(i)$ and $X_l(j)$, where $i \neq j$. This dissimilarity measure reflects how similar or different two temporal sequences are, based on a chosen threshold r. SampEn is then computed as follows:

$$\mathrm{SampEn} = -\ln \frac{A}{B}$$

where A is the number of template vector pairs (i, j) such that the distance between their extended template vectors of length $l + 1$, $X_{l+1}(i)$ and $X_{l+1}(j)$, is less than a tolerance r, i.e., $\mathscr{D}[X_{l+1}(i), X_{l+1}(j)] < r$, B is the number of template vector pairs (i, j) such that the distance between their original template vectors of length l, $X_l(i)$ and $X_l(j)$, is less than r, i.e., $\mathscr{D}[X_l(i), X_l(j)] < r$.

For fMRI time series, SampEn measures the regularity and complexity of brain activity across time. A low SampEn value indicates more regular or predictable brain activity, while a high value reflects more complex and less predictable activity. This measure is particularly useful for studying spontaneous brain activity during rsfMRI, as it quantifies the temporal structure and dynamic behavior of the signal.

2.4 Spatial Correlation Analysis of Brain Entropy Alterations with Neurotransmitter Density Profiles and Cell-Type Distribution Maps

The selected set of 30 neurotransmitter and metabolic maps, derived from positron emission tomography (PET), single-photon emission computed tomography (SPECT), and MRI (including arterial spin labeling-derived cerebral blood flow, ASL_CBF), included receptor and transporter subtypes such as 5-hydroxytryptamine (serotonin, 5HT) receptors ($5HT_{1a}$ [13, 14], $5HT_{1b}$ [13], $5HT_{2a}$ [13], $5HT_4$ [14], $5HT_6$ [15]), cannabinoid receptor type 1 (CB1) [16], cerebral blood flow (CBF) [17], dopamine receptors (D1 [18], D2 [19]), 6-[^{18}F]fluoro-L-DOPA (FDOPA) [20], dopamine transporter (DAT) [21], noradrenaline transporter (NAT) [22], gamma-aminobutyric acid type A receptors ($GABA_a$ [21], $GABA_{a5}$ [23]), mu-opioid receptor (MU, MOR) [24], N-methyl-D-aspartate receptor (NMDA) [25], serotonin transporter (SERT) [26, 13, 14], metabotropic glutamate receptor 5 (mGluR5) [5], vesicular acetylcholine transporter (VAChT) [5], nicotinic acetylcholine receptor $\alpha 4\beta 2$ subtype (A4B2) [27], cerebral metabolic rate of glucose consumption (CMRglu) [28], cyclooxygenase-1 (COX1) [29], histone deacetylase (HDAC) [30], kappa-opioid receptor (KOR) [31], muscarinic acetylcholine receptor M1 (M1) [32], microglial marker (Microglia) [33], synaptic vesicle glycoprotein 2A (SV2A) [34], and vesicular monoamine transporter type 2 (VMAT2) [35]. The neurotransmitter maps are available at https://github.com/netneurolab/hansen_receptors.

In addition to neurotransmitter and metabolic density maps, we incorporated a comprehensive set of 18 cell-type and 6 mitochondrial function distribution maps to further investigate the biological basis of brain entropy alterations. These maps, derived from transcriptomic and histological data in healthy human brain tissue, capture the spatial distribution of various glial, neuronal, and mitochondrial components. The glial maps [6] include astrocytes (Glia-Astro), endothelial cells (Glia-Endo), microglia (Glia-Micro), oligodendrocyte precursor cells (Glia-OPC), and mature oligodendrocytes (Glia-Oligo). Mitochondrial function [8] is represented by maps reflecting enzymatic activity and metabolic capacity, including Complex I (NADH), Complex II (succinate dehydrogenase, SDH), Complex IV (cytochrome c oxidase, COX),

overall respiratory capacity, tissue density, and tissue-specific respiratory capacity (these maps can be accessed at https://neurovault.org/collections/16418/). Neuronal cell-type maps [7] encompass both excitatory and inhibitory subpopulations. Excitatory neuron subtypes (e.g., Ex1–Ex7) are defined based on their projection targets and laminar location, while inhibitory interneurons are categorized by molecular markers such as vasoactive intestinal peptide (VIP), somatostatin (SST), reelin (RELN), neuronal-derived neurotrophic factor (NDNF), cholecystokinin (CCK), parvalbumin (PVALB), and nitric oxide synthase (NOS). These cell-type and mitochondrial maps were selected for their capacity to capture detailed cellular and metabolic heterogeneity across the human cortex, thereby offering key insights into the potential cellular mechanisms contributing to altered entropy patterns observed in neuropsychiatric disorders.

2.5 Statistical Analysis

To quantify the magnitude of group differences in brain entropy between diagnostic groups, we computed voxel-wise Cohen's d effect size maps. This analysis was performed across all voxels to produce spatial maps that reflect the extent of entropy alterations between groups. Positive d values indicate higher entropy in one group relative to the other, while negative values indicate the opposite. These spatial effect size maps offer a detailed view of how intrinsic brain activity complexity varies across psychosis-spectrum conditions and highlight brain regions most affected in each comparison.

Furthermore, Spearman correlation analysis was conducted to examine the associations between brain entropy alterations extracted using the Neuromorphometrics atlas (https://github.com/neurodebian/spm12/tree/master/tpm) and the spatial distributions of neurotransmitter and cell-type values mapped using the same atlas. Comparisons were made across diagnostic groups, and Spearman correlation coefficients (Fisher's z-transformed) were computed between z-scored brain entropy alteration maps and each selected neurotransmitter or cell-type distribution map.

3 Experimental Results

3.1 Brain Entropy, Neurotransmitter, and Cellular Expression Values in the Brain

As shown in Fig.1, voxel-wise SampEn was first estimated from preprocessed resting-state fMRI data collected from a large cohort of subjects. These voxel-level estimates were then parcellated into regional values using the Neuromorphometrics atlas. In parallel, 30 neurotransmitter density maps and 24 cellular distribution maps were processed. The cellular maps encompassed various neuronal and glial subtypes, as well as mitochondrial markers. All maps were registered and resampled to MNI space to ensure alignment with the fMRI data. Regional values for neurotransmitter and cellular features were extracted using the same anatomical atlas to facilitate consistent spatial comparisons across modalities.

3.2 Voxel-wise Brain Entropy Effect Size Maps Across Psychosis

We quantified differences in brain entropy across diagnostic groups by computing voxel-wise effect size maps using Cohen's d. Specifically, pairwise comparisons were performed between NC and SZ, NC and BP, and SZ and BP. As illustrated in Fig.2, we observed that the orbitofrontal cortex exhibits higher SampEn in SZ, which reflects increased complexity and irregularity in neural activity. This heightened entropy indicates less predictability in the temporal patterns of brain activity, suggesting that the neural signals in this region become more disordered or variable. In simpler terms, the higher entropy suggests that the brain is experiencing a greater degree of uncertainty or fluctuation in its functional state, which may be a result of dysfunctional neural processing. These irregularities in neural activity may be linked to impairments in cognitive functioning. Notably, this finding closely aligns with prior clinical studies [36], which have documented comparable alterations in the orbitofrontal cortex among individuals with SZ, thereby strengthening the evidence for its critical role in the pathophysiology of SZ and related psychiatric conditions, including BP. In the case of BP, we also observed pronounced increases in sample entropy within the visual cortex, suggesting heightened neural complexity and dysregulation in sensory processing regions that may reflect disorder-specific neural dynamics.

In addition, given the substantial clinical overlap between SZ and BP, distinguishing between these two conditions remains a significant challenge. However, our SampEn analysis revealed that the orbitofrontal cortex exhibits markedly stronger differences between SZ and BP, suggesting that this region may serve as a promising neural marker for differentiating these clinically similar disorders.

3.3 Brain Entropy Alterations in Relation to Neurotransmitter and Metabolic Distributions

As shown in Fig.3***A***, the 30 neurotransmitter maps were plotted to visualize the spatial distribution of neurotransmitter expression across the brain. In Fig.3***B***, we show SampEn alterations showed significant spatial correlations with several neurotransmitter distributions across diagnostic comparisons. In patients with SZ relative to NC, SampEn alterations were significantly associated with the spatial distribution of dopamine receptor (D1) (r = -0.044, p = 0.030), mu-opioid receptors (MOR; r = -0.052, p = 0.015), and MU receptors (r = -0.051, p = 0.014), all surviving false discovery rate (FDR) correction at $p < 0.05$. This result is particularly interesting and aligns well with previous clinical studies, which have demonstrated that in SZ, both dopamine and mu-opioid receptor systems play crucial roles, with consistent evidence indicating alterations in their function and availability [37, 38].

Similarly, in BP patients relative to NC, SampEn alterations were significantly correlated with the spatial distribu-

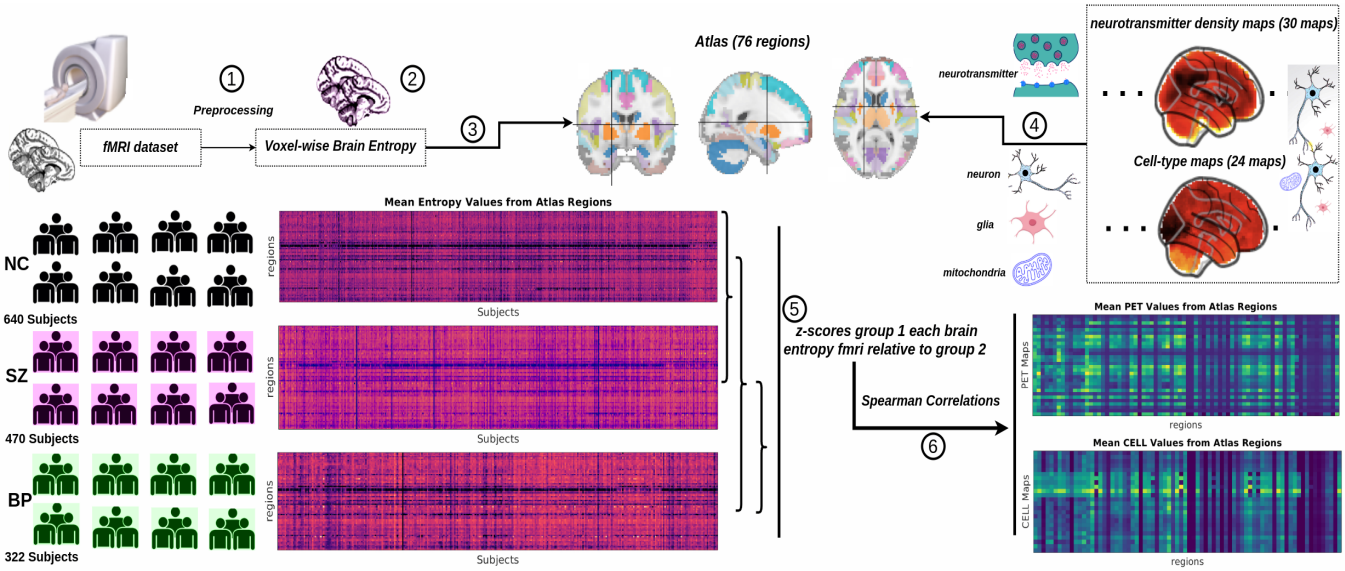

Fig. 1: **Analysis pipeline.** Raw fMRI data from NC, SZ, and BP participants were first preprocessed, followed by voxel-wise brain entropy estimation using SampEn. Mean brain entropy values were then extracted from 76 regions defined by the Neuromorphometrics atlas for each group. In parallel, mean values were also extracted from 30 neurotransmitter maps (derived from PET) and 24 cell-type expression maps, including 18 neuronal and glial cell-type maps and 6 maps representing mitochondrial function. Next, z-scores of brain entropy differences between groups (e.g., NC vs. SZ) were computed. Finally, Spearman correlations were performed between group-level brain entropy alterations and molecular (PET) and cellular (cell-type) maps to identify biologically relevant group differences.

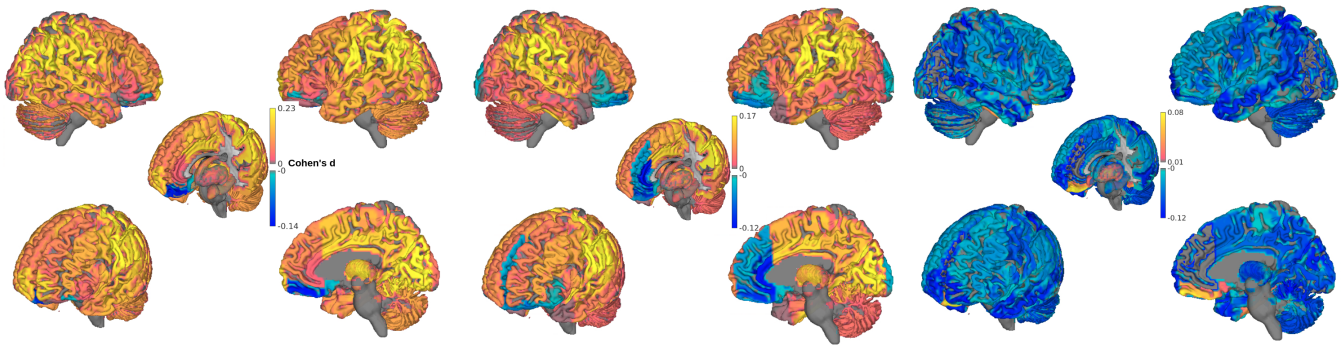

Fig. 2: **Effect size maps across psychosis.** Brain entropy effect sizes were calculated for each pairwise group comparison: NC vs. SZ, NC vs. BP, and SZ vs. BP. The resulting Cohen's d values were mapped back onto brain surface to visualize which brain regions exhibited the strongest effects.

tion of noradrenaline transporters (NAT; $r = 0.058$, $p = 0.029$) and NMDA receptors ($r = 0.052$, $p = 0.030$), with all results FDR-corrected at $p < 0.05$. This finding is consistent with clinical studies, which have also demonstrated a strong link between these receptors and the pathophysiology of BP [39, 40]. These alterations in receptor function may contribute to the clinical manifestation and progression of the disorder, providing further evidence of the neurobiological underpinnings of BP.

However, no significant correlations between SampEn alterations and neurotransmitter distributions were observed in the SZ versus BP comparison.

3.4 Brain Entropy Alterations in Relation to Cellular-Type Maps

As shown in Fig. 4***A***, the spatial distribution of cell-type expression across the brain was visualized using 24 cell-type distribution maps, encompassing neuronal, glial, and mitochondrial cell types. In Fig.4***B***, alterations in SampEn demonstrated significant spatial correlations with several cell-type distributions across diagnostic groups. In patients with SZ compared to NC, SampEn alterations were significantly associated with

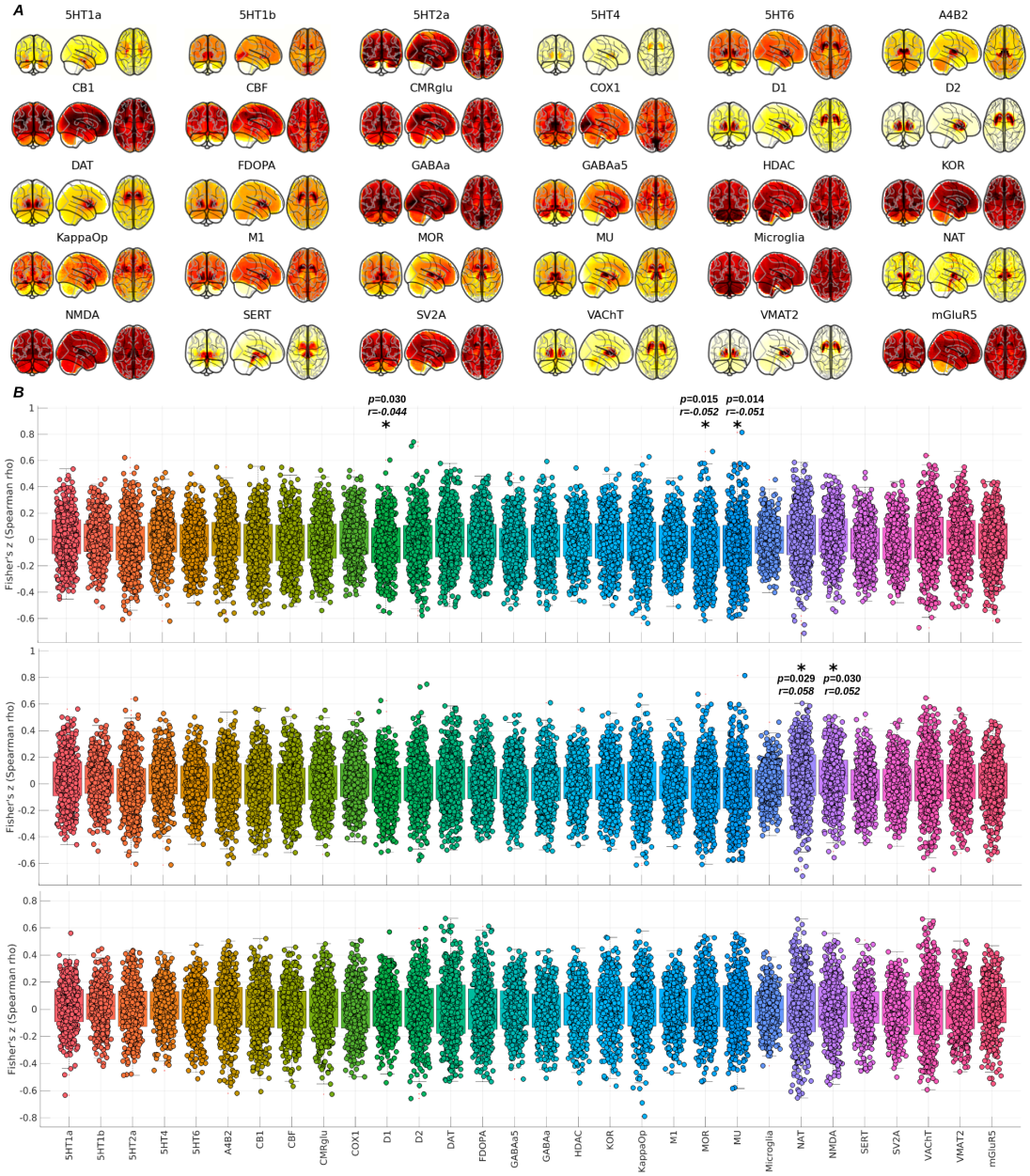

Fig. 3: **Results of spatial correlation analyses between brain entropy alterations and neurotransmitter/metabolic distribution.** ***A.*** Thirty neurotransmitter and metabolic density maps. ***B.*** Spatial correlation results based on the Neuromorphometrics atlas. From top to bottom, the rows show brain entropy alterations for NC vs. SZ, NC vs. BP, and SZ vs. BP. These alterations are voxel-wise correlated with each neurotransmitter/metabolic map. Significant relationships are denoted by * ($p < 0.05$, FDR-corrected).

the spatial distribution of mitochondria and glial cells, particularly astrocytes (Glia-Astro; r = -0.030, p = 0.024), as well as inhibitory neurons, including neuron-In1-VIP-RELN-NDNF-L12 (r = -0.038, p = 0.019) and neuron-In4-RELN-NDNF-L13 (r = 0.039, p = 0.019). These findings suggest that the altered brain signal complexity in SZ may be linked to disruptions in energy metabolism, neuroinflammatory processes, and inhibitory neurotransmission. Meanwhile, these findings provide a biological foundation for brain entropy, supporting its potential utility as a proxy marker for underlying cellular dysfunction and as a quantitative index for characterizing neuropathological changes in SZ.

In addition to findings in patients with SZ, patients with BP relative to NC also exhibited a similar pattern, in which Sam-

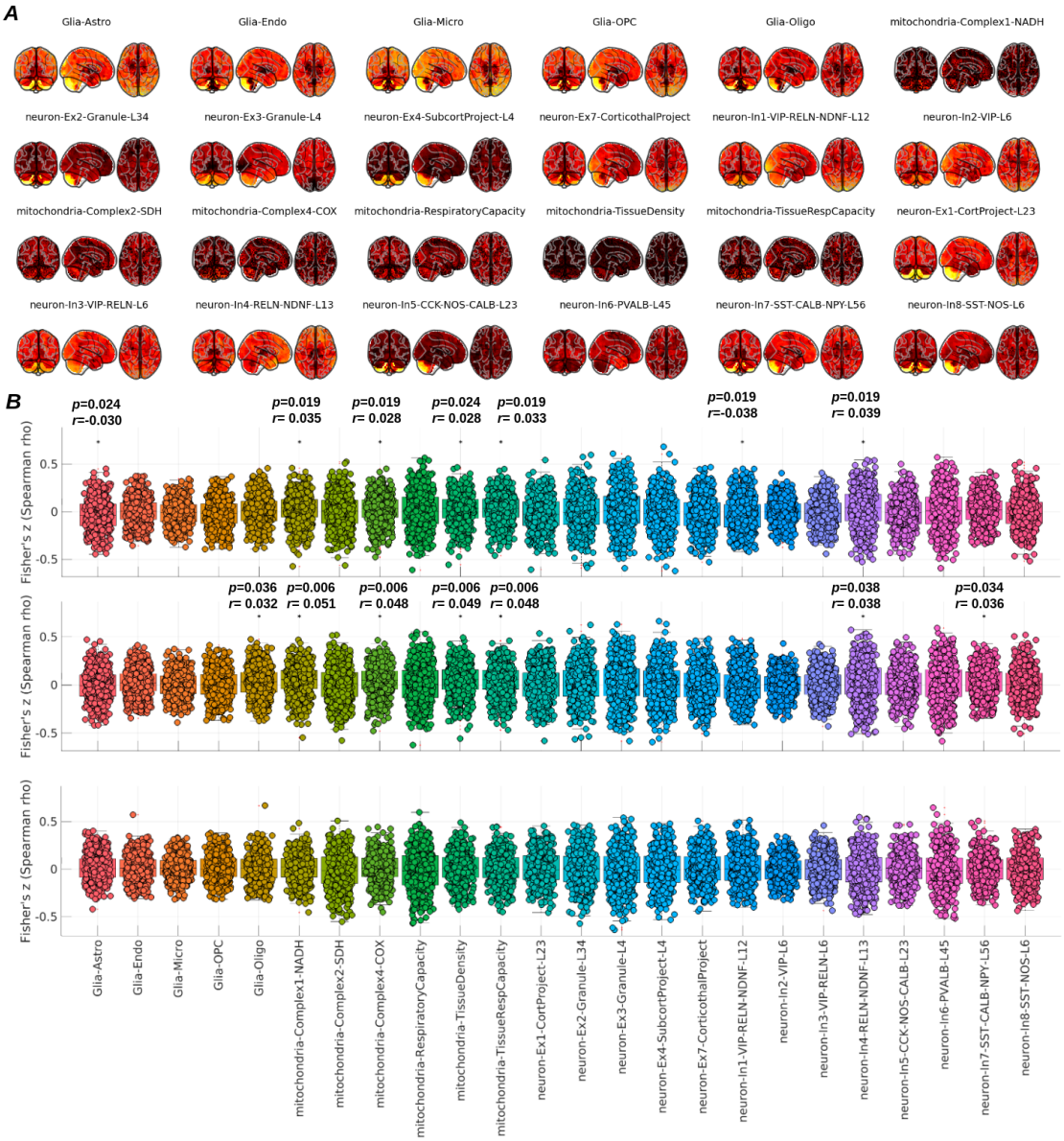

Fig. 4: **Results of spatial correlation analyses between brain entropy alterations and cell-type distribution.** ***A.*** Twenty-four cell-type maps. ***B.*** Spatial correlation results based on the Neuromorphometrics atlas. From top to bottom, the rows show brain entropy alterations for NC vs. SZ, NC vs. BP, and SZ vs. BP. These alterations are voxel-wise correlated with each cell-type map. Significant relationships are denoted by an asterisk (*; $p < 0.05$, FDR-corrected).

pEn alterations were significantly correlated with the spatial distribution of most mitochondrial cell types and neuron-In4-RELN-NDNF-L13 ($r = 0.038$, $p = 0.038$). This common pattern suggests that both SZ and BP may involve disruptions in energy metabolism at the cellular level. Furthermore, SampEn alterations in BP were also significantly associated with the spatial distribution of oligodendrocytes (Glia-Oligo; $r = 0.032$, $p = 0.036$), indicating potential involvement of myelination-related processes. These results further imply that SZ and BP share overlapping pathophysiological features, particularly related to mitochondrial dysfunction, neuroinflammatory activity, and inhibitory neuronal regulation.

Furthermore, no significant correlations between SampEn alterations and cell-type distributions were observed in the SZ versus BP comparison.

3.5 Identifying Key Neurotransmitter and Cell Type Associations with SampEn Alterations

As shown in Fig.5, to facilitate a better comparison of the relationships between SampEn alterations and the spatial dis-

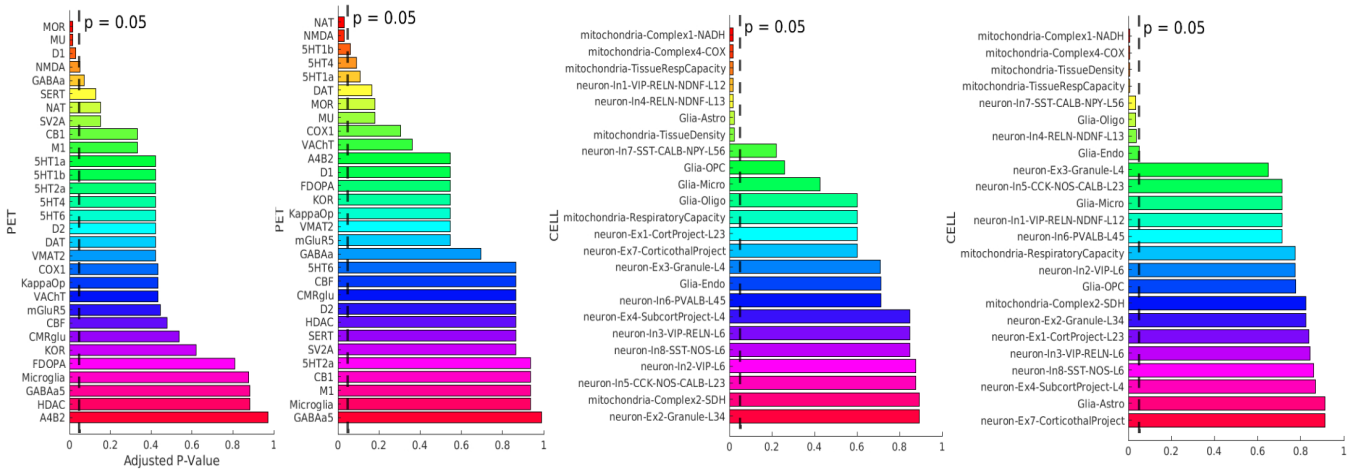

Fig. 5: **Spatial Distribution of SampEn Alterations in Relation to Neurotransmitter and Cell Type Expression.** From left to right, the figure shows the spatial correlations between SampEn alterations (NC vs. SZ and NC vs. BP) and the distributions of neurotransmitters and cell types. Significant associations ($p < 0.05$, FDR corrected) are labeled accordingly.

tributions of neurotransmitters and cell types, we plotted all FDR-corrected p-values in ascending order. Features exhibiting significant associations ($p < 0.05$) were highlighted and labeled accordingly. This visualization enhances the comparison of effect strengths across different features, enabling the identification of the most strongly associated neurotransmitters and cell types contributing to entropy alterations.

4 Limitations of the Study

One limitation of this study is the reliance on a relatively low-resolution brain atlas, despite the availability of higher-resolution atlases that could offer more detailed spatial information and improve the accuracy of observed spatial distributions; incorporating data-driven or hybrid atlases, such as NeuroMark [41], could further enhance these analyses. Second, the analysis does not incorporate transcriptomic data, which would allow for a more comprehensive understanding of gene expression patterns and their relationship to brain entropy alterations. Third, the study focuses primarily on pairwise interactions between SampEn alterations and cell-type distributions, and does not explore higher-order interactions [42], which could reveal more complex relationships and offer deeper insights into the brain's cellular architecture. Fourth, the analysis of neurotransmitter and cell-type distributions is constrained by the current resolution and specificity of available maps, which may not fully capture the diversity and dynamic changes of these populations across different brain regions. Finally, this study only examines static brain entropy, whereas dynamic brain entropy might offer more nuanced insights into the temporal fluctuations and network interactions that underlie brain activity. These limitations suggest that future studies incorporating higher-resolution atlases, transcriptomic data, higher-order interactions, and dynamic entropy measures could further enhance our understanding of the neurobiological mechanisms involved in disorders such as schizophrenia and bipolar disorder.

5 Conclusion

This study bridges the gap between brain entropy and the molecular and cellular architecture of the brain, providing a deeper understanding of psychosis. Moving beyond traditional macro-level approaches, we now explore the intricate relationships at the neurotransmitter and cellular levels. This shift offers a more nuanced perspective on the biological mechanisms underlying psychosis, enhancing our understanding of its manifestation at both systemic and cellular scales. Significant entropy correlations were found in psychosis, linked to several neurotransmitter systems. Additionally, we observed disruptions in energy metabolism, neuroinflammation, and inhibitory neuronal regulation, particularly at the cellular level, in mitochondrial markers. These findings highlight that brain entropy is systematically connected to specific neurochemical systems and cellular features, offering new insights into the biological mechanisms of psychosis.

6 Declaration of Competing Interest

The authors declare that they have no known competing financial interests or personal relationships that could have appeared to influence the work reported in this paper.

7 Authorship Contribution Statement

Qiang Li: Writing – original draft, Visualization, Validation, Software, Methodology, Investigation, Formal analysis. Jingyu Liu: Writing – review & editing, Funding acquisition, Resources, Methodology. Vince D. Calhoun: Writing – review & editing, Funding acquisition, Resources, Methodology.

8 Acknowledgements

This work was supported by NSF grant 2112455.

9 References

[1] J. S. Richman and J. R. Moorman, "Physiological time-series analysis using approximate entropy and sample entropy," *American Journal of Physiology-Heart and Circulatory Physiology*, vol. 278, no. 6, pp. H2039–H2049, 2000.

[2] Z. Wang, Y. Li, A. R. Childress, and J. A. Detre, "Brain entropy mapping using fmri," *PLOS ONE*, vol. 9, pp. 1–8, 03 2014.

[3] Q. Li, M. Seraji, V. D. Calhoun, and A. Iraji, "Complexity measures of psychotic brain activity in the fmri signal," in *2024 IEEE Southwest Symposium on Image Analysis and Interpretation (SSIAI)*, pp. 9–12, 2024.

[4] Q. Li, J. Liu, G. D. Pearlson, J. Chen, Y.-P. Wang, J. A. Turner, and V. D. Calhoun, "Spatiotemporal complexity in the psychotic brain," *bioRxiv:10.1101/2025.01.14.632764*, 2025.

[5] J. Hansen, G. Shafiei, R. Markello, K. Smart, S. Cox, M. Nørgaard, V. Beliveau, Y. Wu, J. Gallezot, É. Aumont, S. Servaes, S. Scala, J. DuBois, G. Wainstein, G. Bezgin, T. Funck, T. Schmitz, R. Spreng, M. Galovic, M. Koepp, J. Duncan, J. Coles, T. Fryer, F. Aigbirhio, C. McGinnity, A. Hammers, J. Soucy, S. Baillet, S. Guimond, J. Hietala, M. Bedard, M. Leyton, E. Kobayashi, P. Rosa-Neto, M. Ganz, G. Knudsen, N. Palomero-Gallagher, J. Shine, R. Carson, L. Tuominen, A. Dagher, and B. Misic, "Mapping neurotransmitter systems to the structural and functional organization of the human neocortex," *Nature Neuroscience*, vol. 25, pp. 1569–1581, November 2022.

[6] S. Darmanis, S. A. Sloan, Y. Zhang, M. Enge, C. Caneda, L. M. Shuer, M. G. Hayden Gephart, B. A. Barres, and S. R. Quake, "A survey of human brain transcriptome diversity at the single cell level," *Proceedings of the National Academy of Sciences of the United States of America (PNAS)*, vol. 112, no. 23, pp. 7285–7290, 2015.

[7] B. B. Lake and et al., "Neuronal subtypes and diversity revealed by single-nucleus rna sequencing of the human brain," *Science*, 2016.

[8] E. V. Mosharov, A. M. Rosenberg, A. S. Monzel, and M. Picard, "A human brain map of mitochondrial respiratory capacity and diversity," *Nature*, vol. 632, no. 7998, pp. 478–485, 2025.

[9] N. S. Rawani, A. W. Chan, S. M. Dursun, and G. B. Baker, "The underlying neurobiological mechanisms of psychosis: Focus on neurotransmission dysregulation, neuroinflammation, oxidative stress, and mitochondrial dysfunction," *Antioxidants*, vol. 13, no. 6, p. 709, 2024.

[10] R. Brisch, A. Saniotis, R. Wolf, H. Bielau, H. Bernstein, J. Steiner, B. Bogerts, K. Braun, Z. Jankowski, J. Kumaratilake, M. Henneberg, and T. Gos, "The role of dopamine in schizophrenia from a neurobiological and evolutionary perspective: old fashioned, but still in vogue," *Frontiers in Psychiatry*, vol. 5, p. 47, May 2014.

[11] C. A. Tamminga, G. Pearlson, M. Keshavan, J. Sweeney, B. Clementz, and G. Thaker, "Bipolar and schizophrenia network for intermediate phenotypes: Outcomes across the psychosis continuum," *Schizophrenia Bulletin*, vol. 40, pp. S131–S137, 02 2014.

[12] S. Meda, G. Ruaño, A. Windemuth, K. O'Neil, C. Berwise, S. Dunn, L. Boccaccio, B. Narayanan, M. Kocherla, E. Sprooten, M. Keshavan, C. Tamminga, J. Sweeney, B. Clementz, V. Calhoun, and G. Pearlson, "Multivariate analysis reveals genetic associations of the resting default mode network in psychotic bipolar disorder and schizophrenia," *Proceedings of the National Academy of Sciences of the United States of America*, vol. 111, 04 2014.

[13] M. Savli, A. Bauer, M. Mitterhauser, Y.-S. Ding, A. Hahn, T. Kroll, A. Neumeister, D. Haeusler, J. Ungersboeck, S. Henry, S. A. Isfahani, F. Rattay, W. Wadsak, S. Kasper, and R. Lanzenberger, "Normative database of the serotonergic system in healthy subjects using multi-tracer pet," *NeuroImage*, vol. 63, no. 1, pp. 447–459, 2012.

[14] V. Beliveau, M. Ganz, L. Feng, B. Ozenne, L. Højgaard, P. M. Fisher, C. Svarer, D. N. Greve, and G. M. Knudsen, "A high-resolution in vivo atlas of the human brain's serotonin system," *Journal of Neuroscience*, vol. 37, no. 1, pp. 120–128, 2017.

[15] R. Radhakrishnan, N. Nabulsi, E. Gaiser, J.-D. Gallezot, S. Henry, B. Planeta, S.-f. Lin, J. Ropchan, W. Williams, E. Morris, D. C. D'Souza, Y. Huang, R. E. Carson, and D. Matuskey, "Age-related change in 5-ht6 receptor availability in healthy male volunteers measured with 11c-gsk215083 pet," *Journal of Nuclear Medicine*, vol. 59, no. 9, pp. 1445–1450, 2018.

[16] H. Laurikainen, L. Tuominen, M. Tikka, H. Merisaari, R.-L. Armio, E. Sormunen, F. Borgan, M. Veronese, O. Howes, M. Haaparanta-Solin, O. Solin, and J. Hietala, "Sex difference in brain cb1 receptor availability in man," *NeuroImage*, vol. 184, pp. 834–842, 2019.

[17] S. Holiga, F. Sambataro, C. Luzy, G. Greig, N. Sarkar, *et al.*, "Test-retest reliability of task-based and resting-state blood oxygen level dependence and cerebral blood flow measures," *PLOS ONE*, vol. 13, no. 11, p. e0206583, 2018.

[18] S. Hesse, M. Rullmann, J. Luthardt, J. Girbardt, P. Meyer, P. Werner, T. Fritz, O. Sabri, and S. Kaller, "Test–retest measurements of dopamine d1-type receptors using simultaneous pet/mri imaging," *European Journal of Nuclear Medicine and Molecular Imaging*, vol. 44, no. 6, pp. 1025–1032, 2017.

[19] K. Alakurtti, J. J. Johansson, J. Joutsa, and et al., "Long-term test–retest reliability of striatal and extrastriatal dopamine d2/3 receptor binding: Study with [^{11}c]raclopride and high-resolution pet," *Journal of Cerebral Blood Flow & Metabolism*, vol. 35, no. 7, pp. 1199–1205, 2015.

[20] F. J. García-Gómez, J. Lojo-Ramírez, I. Huertas, and D. García-Solís, "Elaboración de una plantilla de spm para la normalización de imágenes de pet con [^{18}f]-dopa," *Imagen Diagnóstica*, vol. 9, pp. 23–25, 09 2018.

[21] J. Dukart, S. Holiga, C. Chatham, and et al., "Cerebral blood flow predicts differential neurotransmitter activity," *Scientific Reports*, vol. 8, p. 4074, 2018.

[22] S. Hesse, G. A. Becker, M. Rullmann, A. Bresch, J. Luthardt, M. K. Hankir, F. Zientek, G. Reißig, M. Patt, K. Arelin, D. Lobsien, U. Müller, S. Baldofski, P. M. Meyer, M. Blüher, M. Fasshauer, W. K. Fenske, M. Stumvoll, A. Hilbert, Y. S. Ding, and O. Sabri, "Central noradrenaline transporter availability in highly obese, non-depressed individuals," *European Journal of Nuclear Medicine and Molecular Imaging*, vol. 44, no. 6, pp. 1056–1064, 2017.

[23] P. B. Lukow, D. Martins, M. Veronese, and et al., "Cellular and molecular signatures of in vivo imaging measures of gabaergic neurotransmission in the human brain," *Communications Biology*, vol. 5, p. 372, 2022.

[24] O. Turtonen, A. Saarinen, L. Nummenmaa, L. Tuominen, M. Tikka, R.-L. Armio, A. Hautamäki, H. Laurikainen, O. Raitakari, L. Keltikangas-Järvinen, and J. Hietala, "Adult attachment system links with brain mu opioid receptor availability in vivo," *Biological Psychiatry: Cognitive Neuroscience and Neuroimaging*, vol. 6, no. 3, pp. 360–369, 2021.

[25] M. Galovic, A. Al-Diwani, U. Vivekananda, and et al., "In vivo n-methyl-d-aspartate receptor (nmdar) density as assessed using positron emission tomography during recovery from nmdar-antibody encephalitis," *JAMA Neurology*, vol. 80, no. 2, pp. 211–213, 2023.

[26] P. Fazio, M. Schain, K. Varnäs, C. Halldin, L. Farde, and A. Varrone, "Mapping the distribution of serotonin transporter in the human brainstem with high-resolution pet: Validation using postmortem autoradiography data," *NeuroImage*, vol. 133, pp. 313–320, 2016.

[27] A. Hillmer, I. Esterlis, J. Gallezot, F. Bois, M. Zheng, N. Nabulsi, S. Lin, R. Papke, Y. Huang, O. Sabri, R. Carson, and K. Cosgrove, "Imaging of cerebral $\alpha 4\beta 2^*$ nicotinic acetylcholine receptors with (-)-[^{18}f]flubatine pet: Implementation of bolus plus constant infusion and sensitivity to acetylcholine in human brain," *NeuroImage*, vol. 141, pp. 71–80, 2016.

[28] G. Castrillon and et al., "An energy costly architecture of neuromodulators for human brain evolution and cognition," *Science Advances*, vol. 9, p. eadi7632, 2023.

[29] M. J. Kim, J. H. Lee, F. Juarez Anaya, and et al., "First-in-human evaluation of [^{11}c]ps13, a novel pet radioligand, to quantify cyclooxygenase-1 in the brain," *European Journal of Nuclear Medicine and Molecular Imaging*, vol. 47, pp. 3143–3151, 2020.

[30] H. Y. Wey and et al., "Insights into neuroepigenetics through human histone deacetylase pet imaging," *Science Translational Medicine*, vol. 8, no. 351, p. 351ra106, 2016.

[31] J. Dukart, S. Holiga, M. Rullmann, R. Lanzenberger, P. C. Hawkins, M. A. Mehta, S. Hesse, H. Barthel, O. Sabri, R. Jech, *et al.*, "Juspace: A tool for spatial correlation analyses of magnetic resonance imaging data with nuclear imaging derived neurotransmitter maps," tech. rep., Wiley Online Library, 2021.

[32] M. Naganawa, N. Nabulsi, S. Henry, D. Matuskey, S.-F. Lin, L. Slieker, A. J. Schwarz, N. Kant, C. Jesudason, K. Ruley, A. Navarro, H. Gao, J. Ropchan, D. Labaree, R. E. Carson, and Y. Huang, "First-in-human assessment of [^{11}c]-lsn3172176, an m1 muscarinic acetylcholine receptor pet radiotracer," *Journal of Nuclear Medicine*, vol. 62, no. 4, pp. 553–560, 2021.

[33] C. Lois, I. González, D. Izquierdo-García, N. R. Zürcher, P. Wilkens, M. L. Loggia, J. M. Hooker, and H. D. Rosas, "Neuroinflammation in huntington's disease: New insights with [^{11}c]-pbr28 pet/mri," *ACS Chemical Neuroscience*, vol. 9, no. 11, pp. 2563–2571, 2018.

[34] S. J. Finnema, N. B. Nabulsi, J. Mercier, and et al., "Kinetic evaluation and test–retest reproducibility of [^{11}c]ucb-j, a novel radioligand for positron emission tomography imaging of synaptic vesicle glycoprotein 2a in humans," *Journal of Cerebral Blood Flow & Metabolism*, vol. 38, no. 11, pp. 2041–2052, 2017.

[35] B. Larsen, V. Olafsson, F. Calabro, and et al., "Maturation of the human striatal dopamine system revealed by pet and quantitative mri," *Nature Communications*, vol. 11, p. 846, 2020.

[36] M. Nakamura, P. G. Nestor, J. J. Levitt, A. S. Cohen, T. Kawashima, M. E. Shenton, and R. W. McCarley, "Orbitofrontal volume deficit in schizophrenia and thought disorder," *Brain*, vol. 131, no. Pt 1, pp. 180–195, 2008.

[37] A. H. Ashok, J. Myers, T. Reis Marques, E. A. Rabiner, and O. D. Howes, "Reduced mu opioid receptor availability in schizophrenia revealed with [11c]-carfentanil positron emission tomographic imaging," *Nature Communications*, vol. 10, no. 1, p. 4493, 2019.

[38] Y. Okubo, T. Suhara, K. Suzuki, K. Kobayashi, O. Inoue, O. Terasaki, Y. Someya, T. Sassa, Y. Sudo, E. Matsushima, M. Iyo, Y. Tateno, and M. Toru, "Decreased prefrontal dopamine d1 receptors in schizophrenia revealed by pet," *Nature*, vol. 385, no. 6617, pp. 634–636, 1997.

[39] S.-X. Cao, Y. Zhang, X.-Y. Hu, B. Hong, P. Sun, H.-Y. He, H.-Y. Geng, A.-M. Bao, S.-M. Duan, J.-M. Yang, T.-M. Gao, H. Lian, and X.-M. Li, "Erbb4 deletion in noradrenergic neurons in the locus coeruleus induces mania-like behavior via elevated catecholamines," *eLife*, vol. 7, p. e39907, 2018.

[40] E. Ramadan, M. Basselin, J. S. Rao, L. Chang, M. Chen, K. Ma, and S. I. Rapoport, "Lamotrigine blocks nmda receptor-initiated arachidonic acid signalling in rat brain: implications for its efficacy in bipolar disorder," *International Journal of Neuropsychopharmacology*, vol. 15, no. 7, pp. 931–943, 2012.

[41] Y. Du, Z. Fu, J. Sui, S. Gao, Y. Xing, D. Lin, M. Salman, A. Abrol, M. A. Rahaman, J. Chen, L. E. Hong, P. Kochunov, E. A. Osuch, and V. D. Calhoun, "Neuromark: An automated and adaptive ica based pipeline to identify reproducible fmri markers of brain disorders," *NeuroImage: Clinical*, vol. 28, p. 102375, 2020.

[42] Q. Li, G. Ver Steeg, and J. Malo, "Functional connectivity via total correlation: Analytical results in visual areas," *Neurocomputing*, p. 127143, 12 2023.